JACS
JOURNAL OF THE AMERICAN CHEMICAL SOCIETY
Article
Cite This: J. Am. Chem. Soc. XXXX, XXX, XXX−XXX
pubs.acs.org/JACS

Mechanistically Driven Control over Cubane Oxo Cluster Catalysts

Fangyuan Song,[†] Karrar Al-Ameed,[†,‡] Mauro Schilling,[†] Thomas Fox,[†] Sandra Luber,[†] and Greta R. Patzke*[,†]

[†]Department of Chemistry, University of Zurich, Winterthurerstrasse 190, CH-8057 Zurich, Switzerland
[‡]Faculty of Science, University of Kufa, 54001 Najaf, Iraq

Supporting Information

ABSTRACT: Predictive and mechanistically driven access to polynuclear oxo clusters and related materials remains a grand challenge of inorganic chemistry. We here introduce a novel strategy for synthetic control over highly sought-after transition metal $\{M_4O_4\}$ cubanes. They attract interest as molecular water oxidation catalysts that combine features of both heterogeneous oxide catalysts and nature's cuboidal $\{CaMn_4O_5\}$ center of photosystem II. For the first time, we demonstrate the outstanding structure-directing effect of straightforward inorganic counteranions in solution on the self-assembly of oxo clusters. We introduce a selective counteranion toolbox for the controlled assembly of di(2-pyridyl) ketone (dpk) with $M(OAc)_2$ (M = Co, Ni) precursors into different cubane types. Perchlorate anions provide selective access to **type 2** cubanes with the characteristic $\{H_2O\text{-}M_2(OR)_2\text{-}OH_2\}$ edge-site, such as $[Co_4(dpy\text{-}C\{OH\}O)_4(OAc)_2(H_2O)_2](ClO_4)_2$. **Type 1** cubanes with separated polar faces $[Co_4(dpy\text{-}C\{OH\}O)_4(L2)_4]^{n+}$ (L2 = OAc, Cl, or OAc and H_2O) can be tuned with a wide range of other counteranions. The combination of these counteranion sets with $Ni(OAc)_2$ as precursor selectively produces **type 2** Co/Ni-mixed or $\{Ni_4O_4\}$ cubanes. Systematic mechanistic experiments in combination with computational studies provide strong evidence for **type 2** cubane formation through reaction of the key dimeric building block $[M_2(dpy\text{-}C\{OH\}O)_2(H_2O)_4]^{2+}$ with monomers, such as $[Co(dpy\text{-}C\{OH\}O)(OAc)(H_2O)_3]$. Furthermore, both experiments and DFT calculations support an energetically favorable **type 1** cubane formation pathway via direct head-to-head combination of two $[Co_2(dpy\text{-}C\{OH\}O)_2(OAc)_2(H_2O)_2]$ dimers. Finally, the visible-light-driven water oxidation activity of **type 1** and **2** cubanes with tuned ligand environments was assessed. We pave the way to efficient design concepts in coordination chemistry through ionic control over cluster assembly pathways. Our comprehensive strategy demonstrates how retrosynthetic analyses can be implemented with readily available assembly directing counteranions to provide rapid access to tuned molecular materials.

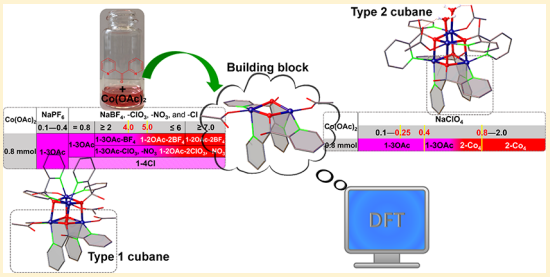

INTRODUCTION

The present global health energy and challenges trigger an increasing demand for new functional inorganic compounds and catalysts. In sharp contrast, their formation mechanisms and truly predictive syntheses remain grand challenges of inorganic chemistry. Considerable progress has been reported in computer-aided solid state and organic synthesis,[1−3] and major progress in synthetic coordination chemistry is expected from forthcoming machine learning approaches.

Polynuclear transition metal-oxo complexes and polyoxometalates are prominent targets in current catalytic, bioinorganic, medicinal, and materials research.[4−6] Their wide application range encompasses, for example, catalytic water splitting,[7−12] new antimicrobial agents,[13] and single molecule magnets.[14] However, they also embody the present challenges of predictive coordination chemistry, because the formation pathways of most polynuclear transition metal oxo clusters remain widely unknown. This makes their full exploration and systematic access to all their attractive properties difficult.[15−22]

Here we present an unprecedented level of synthetic control over transition metal cubane oxo clusters that keep attracting interdisciplinary interest, e.g., as catalytic model systems for nature's photosystem II[23] or as magnetic materials.[24,25] We introduce a toolbox of straightforward inorganic counteranions as one-pot and highly efficient structure-directing agents for cubane assembly in aqueous solution. Furthermore, we investigate the underlying formation mechanisms that provide controlled access to a wide spectrum of $\{M_4O_4\}$ (M = Co, Ni, or Co/Ni) cubanes.

Currently, the gap between the growing number of self-assembled metal-oxo clusters on the one hand and the lack of truly predictive design concepts is still widening. Intense investigations into their formation processes are thus required to develop predictive access strategies. Recent progress includes detailed speciation, analytical growth tracking as well as crystallization studies of smaller[18] and larger[26] polyoxometalates. More insight into the influence of self-assembly[27] on oxo cluster formation compared to external

Received: February 4, 2019

DOI: 10.1021/jacs.9b01356
J. Am. Chem. Soc. XXXX, XXX, XXX−XXX

chemical stimuli is now indispensable for convenient toolbox protocols.

The considerable templating and recognition properties of inorganic counteranions emerged from supramolecular chemistry research[28−34] and attracts increasing attention in bio-, environmental, and inorganic chemistry.[31,35−39] However, the full structure-directing potential of counteranions is still far from explored. The majority of synthetic studies are focused on solid state anion template effects on the crystal structure of (oxo) cluster materials,[40] e.g., halide-templated assemblies of first row transition metal ions.[41] Far less is known about anionic structure-directing control over oxo clusters in situ, i.e., during their assembly processes in solution.

Understanding the influence of anions on cluster formation pathways with full computational analyses first requires far more fundamental insight into the basic physicochemical properties of hydrated anions, beyond the present state. In sharp contrast to the well studied hydration behavior of cations, such experimental studies on anions in aqueous solutions still remain quite limited due to the oftentimes very fast exchange rates (ps regime) of their weakly bound water ligands.[42] Structural information on anion environments in solution can be obtained from large angle X-ray or neutron scattering, respectively.[43] The combination of such advanced analyses with simulations of hydrated anionic structures in solution and their water exchange mechanisms[44] currently paves the way to their more comprehensive understanding. Recent illustrative examples include modeling studies on four counteranions used in the present work (ClO_4^-,[45] ClO_3^-,[45] BF_4^-,[46] and hexafluorophosphate[46]).

Transition metal and heterometallic[47−51] cubanes are attractive and sought-after targets for new design approaches in coordination chemistry. They are quite versatile catalytic model systems—both for nature's cuboidal and heterometallic $\{CaMn_4O_5\}$ oxygen evolving complex (OEC) of photosystem II[52−55] and for crucial surface motifs of oxide-based water oxidation catalysts (WOCs).[56−58] While much emphasis has been placed on elucidating the oxygen evolution pathways of synthetic cubane clusters, considerably less is known about their own formation processes.[59−63] Heterometallic cubanes provide particularly excellent opportunities to study synergistic effects in oxide-related as well as in bioinspired molecular catalysts,[64] but their targeted construction remains demanding.[65] To the best of our knowledge, the influence of inorganic anions on the assembly pathways of oxo clusters in solution remains rather unexplored. We here demonstrate the potential of straightforward inorganic anions for predictive access to cubanes, providing inspirational input for forthcoming machine learning approaches.

To this end, model systems with Co(II)- and Ni(II)-salt precursors and di(2-pyridyl) ketone (dpk) as ligand for cubane formation were operated with systematically varied inorganic counteranion types and concentrations. While dpk has been identified as an efficient ligand for transition metal cubane formation in previous studies,[66−69] the overarching, mechanistically driven design of transition metal oxo cluster remains highly sought-after. We first provide a comprehensive roadmap to different types of $\{M_4O_4\}$ cubane oxo clusters and their heterometallic analogues from $M(OAc)_2$/dpk/NaX (M = Co, Ni; X = ClO_4, ClO_3, BF_4, PF_6, NO_3, and Cl) model systems. Furthermore, we proceed to their mechanistic and computational analyses and conclude with key visible-light-driven water oxidation performance data.

RESULTS AND DISCUSSION

Cubane Structures: Type 1 and Type 2. *Structures.* All cubanes discussed in this study belong to two different types (**1** and **2**) with alternative coordination modes of the primary dpy-C{OH}O$^-$ ligand to the $\{M_4O_4\}$ core. The general **type 1** and **type 2** structures and the different accessibilities of their polar faces are illustrated in Figure 1 (CIF files for all cubanes are provided in the SI).

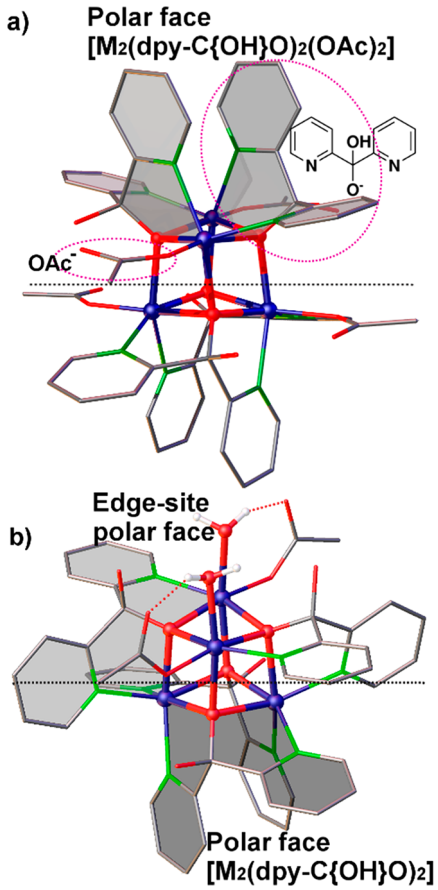

Figure 1. Structural features of **type 1** (a) and **2** (b) cubanes (ligand hydrogen atoms and counteranions are omitted for clarity; Co: dark blue, C: gray, O: red, N: green; inset in (a) = structure of the hydrolyzed dpk ligand).

Nomenclature. For **type 1** cubanes, type and number of secondary ligands (OAc^- and Cl^-) and of their corresponding isolated counteranions are successively abbreviated as in the following example: **1**(*type*)-**3OAc**(*three secondary acetate ligands*)-**BF_4**(*one BF_4^-counteranion*), as in $[Co_4(dpy\text{-}C\{OH\}O)_4(OAc)_3(H_2O)]BF_4$ (cf. also Figure 3c).

For mixed Co/Ni **type 1** cubanes, their general or specifically determined compositions are indicated likewise, such as in **1-Co_xNi_{4-x}-3OAc-NO_3** representing the mixed cubane $[Co_xNi_{4-x}(dpy\text{-}C\{OH\}O)_4(OAc)_3(H_2O)]NO_3$.

In **type 2** cubane compounds, "**μ-OAc**" after the initial **2** refers to the presence of a bridging acetate ligand, followed by "**Co_xNi_{4-x}**" or "**Ni_4**" and the respective counteranion types, e.g., **2-μ-OAc-Co_xNi_{4-x}-ClO_4** abbreviating $[Co_xNi_{4-x}(dpy\text{-}C\{OH\}O)_4(OAc)_2(\mu\text{-}OAc)]ClO_4$ (Figure 2b, right; $\mu = \mu_2$ in the following).

Finally, short names of cubanes with the characteristic $\{H_2O\text{-}Co_2(OR)_2\text{-}OH_2\}$ edge-site motif are given without

DOI: 10.1021/jacs.9b01356
J. Am. Chem. Soc. XXXX, XXX, XXX−XXX

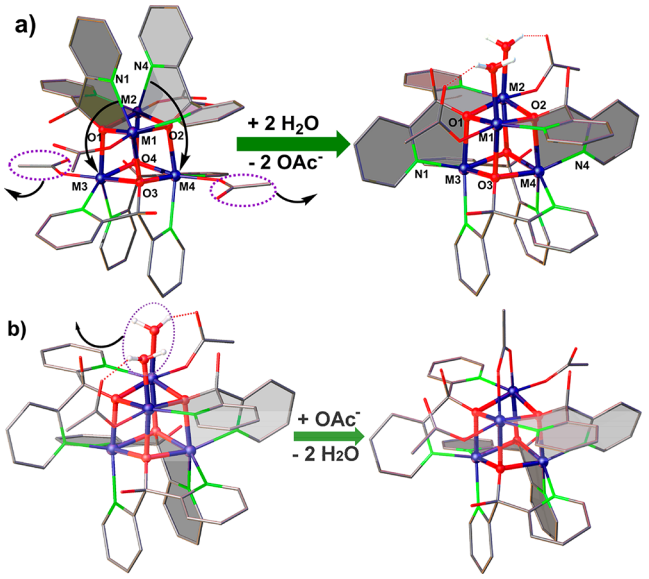

Figure 2. (a) Formal structural transformation from $[M_4(dpy\text{-}C\{OH\}O)_4(OAc)_4]$ (**type 1**) to $[M_4(dpy\text{-}C\{OH\}O)_4(OAc)_2(H_2O)_2]^{2+}$ (**type 2**). (b) Structural transition from cubane cations $[M_4(dpy\text{-}C\{OH\}O)_4(OAc)_2(H_2O)_2]^{2+}$ (2-edge site) to $[M_4(dpy\text{-}C\{OH\}O)_4(OAc)_2(\mu\text{-}OAc)]^{+}$ (**2-μ-OAc**).

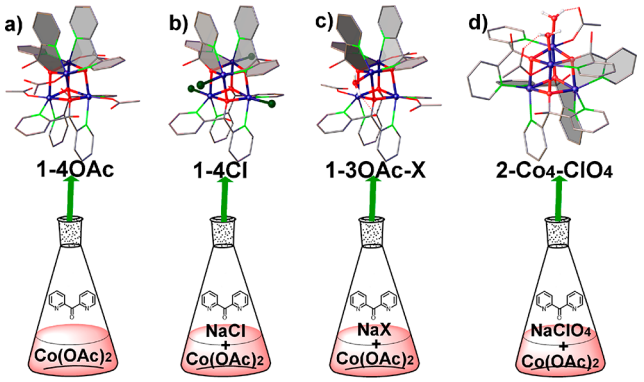

Figure 3. General $\{Co_4O_4\}$ cubane syntheses (a) in the absence of additional counteranions, (b) with Cl^-, (c) in the presence of X^- (X^- = ClO_3^-, NO_3^-, BF_4^-, and PF_6^-), and (d) with ClO_4^-.

explicitly mentioning their "**μ-OAc**" ligands, e.g., **2-Co$_x$Ni$_{4-x}$-BF$_4$** for $[Co_xNi_{4-x}(dpy\text{-}C\{OH\}O)_4(OAc)_2(H_2O)_2](BF_4)_2$ (Figure 2b, left).

Structural Characterization of Type 1 Cubanes. All **type 1** cubanes in the present study were structurally characterized by means of single-crystal X-ray diffraction as well as with select bulk analytical techniques (Tables S1, S2, S9, and Scheme S1). Their cobalt centers are coordinated to three oxygen atoms and two nitrogen atoms of three and two dpy-C{OH}O$^-$ ligands, respectively; in a $\eta{:}^1\eta^3{:}\eta^1$ fashion (Figure S1). Together with a secondary ligand L2, the four octahedrally coordinated cobalt centers form $[Co_4(dpy\text{-}C\{OH\}O)_4(L2)_4]^{n+}$ **type 1** cubanes with two separated polar faces (Figure 1a). Each of them is equipped with two secondary L2 ligands (L2 = monodentate OAc$^-$, monodentate OAc$^-$ and H_2O, and Cl$^-$ for **1-4OAc**, **1-2OAc** and **1-3OAc**, and **1-4Cl**, respectively). The L2 types and ratios can be controlled through selecting appropriate anion types and concentrations during synthesis (cf. Scheme 1, Figure S2 and section below). Systematic replacement of the four acetate ligands of **1-4OAc** with one or two aqua- or four chloride ligands thereby affords the **1-3OAc**, **1-2OAc**, and **1-4Cl** cubanes (Figure 3).

Structural Characterization of Type 2 Cubanes. **Type 2** cubanes were structurally characterized with single-crystal X-ray diffraction throughout, in combination with appropriate bulk analytical techniques (Tables S3–S7, S10–14, and Scheme S1).

2-Edge-Site Cubanes. The upper polar {M-O-M-O} face in the **type 2** cubanes (cf. Figure 1b) bears the secondary ligands (referred to as edge-site in the following), while the lower plane is solely coordinated to dpy-C{OH}O$^-$ ligands (Figure 1b). The formal transition from **type 1** to **type 2** cubanes thus involves the dissociation of two acetate groups (on the same polar side) while recoordinating N1 and N4 to M3 and M4, respectively.

It is completed with the formal addition of an aqua ligand to both M1 and M2 and rotation of the remaining two acetate groups to an approximately perpendicular position facing the {M1O1M2O2} plane (Figure 2a).

2-μ-OAc Cubanes. Furthermore, **type 2** cubanes can be selectively transferred with specific counteranion concentrations (cf. Scheme 1) into their **2-μ-OAc** analogues with bridging acetate groups. This transformation involves replacement of their aqua ligands on the $\{H_2O\text{-}Co_2(OR)_2\text{-}OH_2\}$ edge-site with bidentate acetate ligands, while slightly turning the monodentate acetate ligands toward the adjacent -OH on the same polar faces (Figure 2b). The resulting different position of the monodentate acetate ligand in **2-μ-OAc-Co$_x$Ni$_{4-x}$** (Figures 2b and S7) indicates some positional freedom in the **type 2** cubanes. This also gives rise to the two-component positional disorder of the monodentate acetate moieties in the **2-Co$_x$Ni$_{4-x}$-ClO$_4$**, **-ClO$_3$**, and **-BF$_4$** series (see the corresponding CIF file in the SI for details).

Crystal Packing and Role of the Counteranions. Detailed discussions of anionic disorder, extended hydrogen bonding, and chirality within **type 1** and **type 2** cubanes are given in the SI (cf. p. S28). Most importantly, the anionic positions in their solid state structures do not display substantial differences between the individual cubanes.

Therefore, the selective access to tuned cubane structures as outlined in the following section (cf. Scheme 1) cannot be ascribed to anionic templating in the solid state.

Predictive Anion-Controlled Access to Type 1 and Type 2 Cubanes. *General Synthesis and Characterization.* We have developed a predictive, counteranion-directed access to **type 1** and **type 2** cubanes from the convenient, one-pot reaction of $M(OAc)_2$ as M^{2+} source and dpk as in aqueous solution at room temperature. Scheme 1 illustrates how the experimental protocols for **types 1** and **2** given in the SI (p. S4–S6) can be adjusted with select counteranion concentrations to afford a wide range of cubane targets. The bulk purity of all cubane types obtained from the strategy shown in Scheme 1 was corroborated with four different analytical protocols based on elemental analyses, powder X-ray diffraction (PXRD), ^{1}H NMR and Raman spectroscopy. The choice of these methods is explained in detail in the SI (p. S34–S35, where Scheme S1 specifies the characterization techniques applied to each cubane type). Additionally, further checks of cubane stabilities and Co/Ni-substitution patterns were performed with HR-ESI-MS (cf. p. S30–S34 and

DOI: 10.1021/jacs.9b01356
J. Am. Chem. Soc. XXXX, XXX, XXX–XXX

Scheme 1. Synthetic Fields for Counteranion-Directed Access to Type 1/2 $\{Co_4O_4\}$, $\{Co_xNi_{4-x}O_4\}$, and Type 2 $\{Ni_4O_4\}$ Cubanes[a]

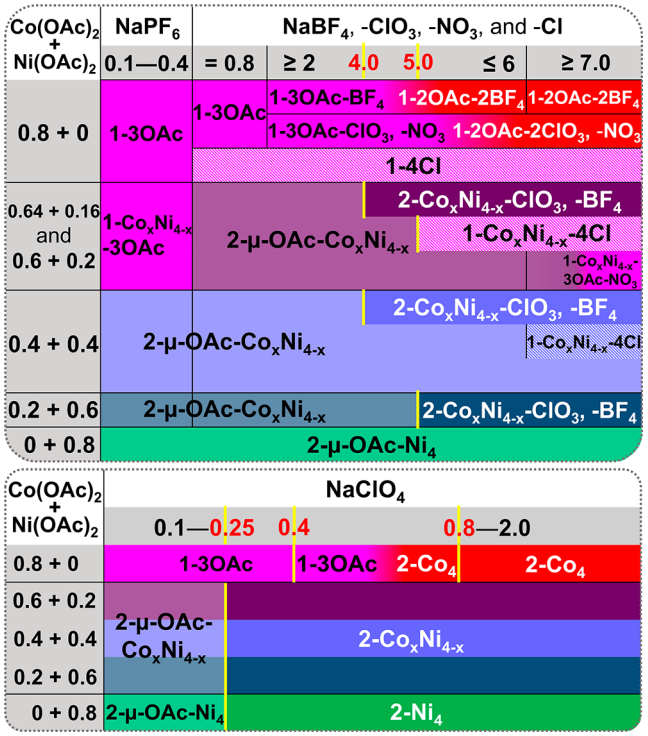

[a]All $M(OAc)_2$ and NaX amounts are given in mmol, referring to the standard experimental procedure provided in the SI. Vertical yellow lines indicate defined NaX concentration thresholds for the respective products (for an overview of analytical characterizations of the products, cf. Scheme S1 in the SI).

S60−S62 in the SI for a complete data evaluation). The level of crystallographic and structural novelty is specified in Table S19 for each of the newly reported cubane structures.

For general synthetic operations and analytical information, we refer to these comprehensive resources in the SI. In the following, we selectively illustrate examples of counteranion control over the different cubane types, which reveal underlying parameters of our new predictive strategy.

Anionic-Directed Access to $\{Co_4O_4\}$ Cubanes. The formation of phase pure edge-site **2-Co_4-ClO_4** in the presence of ≥1.0 equiv ClO_4^- with all initial M^{2+} amounts (cf. also below) served as our starting point[56] to unravel the unprecedented control effect of an entire series of counteranions (ClO_3^-, NO_3^-, BF_4^-, PF_6^-, and Cl^-) on **type 1** $\{Co_4O_4\}$ cubanes (Figure 3d and Scheme 1).

Ligand Tuning of $\{Co_4O_4\}$ Cubanes. As a first representative example for the manifold reactions summarized in Scheme 1, we demonstrate how the number of coordinated acetate ligands can be fine-tuned between **1-3OAc** and **1-2OAc** cubanes with counteranionic control (Scheme 1, upper section).

In the presence of BF_4^-, phase pure **1-3OAc-BF_4** is selectively accessible through addition of 1.0 equiv $NaBF_4$ (Scheme 1 and Figure 3c, cf. Figures S26 and S43a for analytical characterizations). However, a notable increase of the BF_4^- amount to 8.75 equiv reduces the acetate content in the cubane and affords the structural analogue **1-2OAc-2BF_4** (Scheme 1, Figures 4, S4 and S44b, and Table S1 for

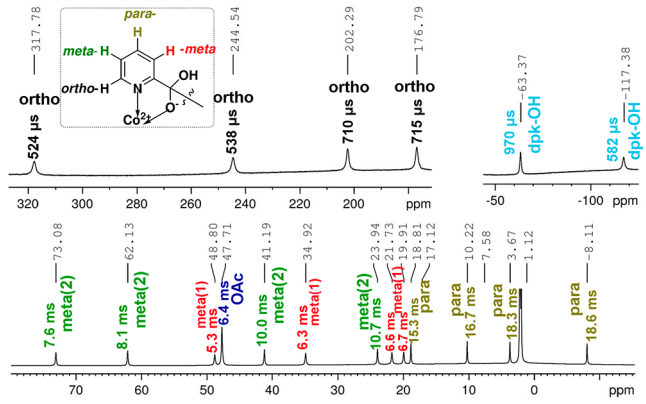

Figure 4. ^1H NMR spectrum of **1-2OAc-2BF_4** and peak assignments on the basis of T1.

crystallographic and analytical data). Consequently, intermediate counteranion amounts of 2.5−7.5 equiv BF_4^- give rise to coexistence of both compounds, as is evident from the presence of both sets of proton signals in the respective ^1H NMR spectra (cf. Figure S27 and Table S15 for the peak assignments). This coexistence of **1-2OAc-2BF_4** and **1-3OAc-BF_4** as products of the intermediate 2.5−7.5 equiv BF_4^- route is evident from the virtually identical ^1H NMR spectrum of a mixture of pure **1-2OAc-2BF_4** and **1-3OAc-BF_4** (Figure S28 and Table S15) compared to that of the as-synthesized mixed product in Figure S27 with corresponding signal intensities.

Anion Selectivity. A related structure-directing effect on the number of associated acetate ligands was observed for systematically varied amounts of NO_3^-, ClO_3^-, and PF_6^- (Scheme 1, Figures S29−S31 and Table S15). In contrast to **1-2OAc-2BF_4**, however, manifold efforts to obtain phase pure **1-2OAc-2NO_3**, **1-2OAc-2ClO_3**, and **1-2OAc-2PF_6** remained unsuccessful so far, as well as attempts to directly access pure **1-2OAc** from saturated sodium salt solutions of these anions. When applying ClO_4^-, a structural transformation from **type 1** to **2** set in for >0.5 equiv $NaClO_4$ (Scheme 1, cf. Figures S32, S33, and Table S16 for the component analysis), and pure **2-Co_4-ClO_4** is accessible with ≥1.0 equiv $NaClO_4$ (Figure S45a).[56]

The exclusive formation of **1-4OAc** from synthetic protocols involving no such counteranions is a strong indication that they indeed control the number of acetate ligands in the **type 1** cubanes through concentration-dependent dissociation processes (Figure 3a, cf. Figure S3a and Table S1 for crystallographic data and Figure S25 for analytical purity).

Furthermore, Cl^- exerts a dual function as both counteranion and ligand that directly coordinates to the cobalt centers. This further extends the above range of **type 1** cubanes with a new, neutral member, namely, $[Co_4(dpy\text{-}C\{OH\}O)_4Cl_4]$, **1-4Cl** (cf. Figures 3b, S3b, and Table S1 for crystallographic data, and Figures 5 and S52a for analytical characterizations).

Access to Heterometallic Co/Ni Cubanes. Scheme 1 furthermore demonstrates how select mixed Co/Ni cubanes can be directly accessed from according $Co(OAc)_2/Ni(OAc)_2$ precursor mixtures and adjusted concentrations of Ni^{2+} and counteranions. All mixed cubanes were checked for bulk purity with the strategies mentioned in the beginning of this section (the detailed techniques are given in Scheme S1).

The formation of genuine mixed **type 1** Co/Ni cubane cores was confirmed with HR-ESI-MS analyses of phase pure, single crystalline samples through applying our previous strategies for

DOI: 10.1021/jacs.9b01356
J. Am. Chem. Soc. XXXX, XXX, XXX−XXX

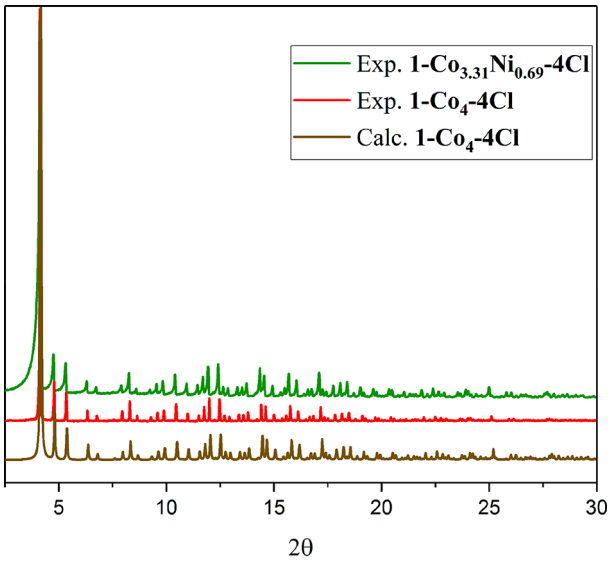

Figure 5. Experimental PXRD patterns of **1-Co_4-4Cl** and **1-$Co_{3.31}Ni_{0.69}$-4Cl** vs the calculated pattern of **1-Co_4-4Cl**.

analyzing **type 2** mixed cubanes.[56] For example, the appearance of isotope patterns at lower *m*/*z* ranges than those of the pure Co containing fragments $[Co_4(dpy\text{-}C\{OH\}O)_4Cl_2]^{2+}$ (*m*/*z* 555^{2+}, Figures S16 and S60) and $[Co_4(dpy\text{-}C\{OH\}O)_4(OAc)_2]^{2+}$ (*m*/*z* 579^{2+}, Figures S15 and S61) indicates the presence of both Ni and Co cations in the cubane cores of **1-Co_xNi_{4-x}-4Cl** and **1-Co_xNi_{4-x}-3OAc-NO_3**, in line with their calculated isotope patterns (Figures S60 and S61).

Synthetic Trends for Co/Ni Cubanes. First, Ni^{2+}/Co^{2+} precursor ratios >1:4 generally afford mixed $\{M_4O_4\}$ cubanes, with a strong preference for **type 2** over **type 1** (Scheme 1 and Figure S2). In the following, we outline that not only the counteranion type but also its concentration exerts a decisive influence on the cubane type.

Counteranion Concentration and 2-μ-OAc-Co/Ni Cubanes. An impressive example for the counteranion influence is the systematic access to a series of **2-μ-OAc-Co_xNi_{4-x}** cubanes with bridging acetate ligands, namely to $[Co_xNi_{4-x}(dpy\text{-}C\{OH\}O)_4(\mu\text{-}OAc)(OAc)_2]ClO_4$, -$ClO_3$, -$NO_3$, -$BF_4$, -$PF_6$, and -Cl with low to moderate counteranion concentrations (Scheme 1, cf. Figure S7 and Table S4 for crystallographic data and Figures S50, S51, and S54 for analytical results). Second, notably increased counteranion concentrations of ClO_4^-, BF_4^-, and ClO_3^- provided direct access to the corresponding edge-site $\{Co_xNi_{4-x}O_4\}$ cubanes, most likely through dissociation of the bridging acetate ligand in **2-μ-OAc-Co_xNi_{4-x}-ClO_4**, **-BF_4**, and **-ClO_3**, respectively (Scheme 1, cf. Figures S6 and Table S3 for the crystallographic data and Figures S45, S47, S48, and S53 for analytical data). This proposed pathway is supported by the spontaneous formation of **2-Co_xNi_{4-x}-PF_6** from as-synthesized **2-μ-OAc-Co_xNi_{4-x}-PF_6** after 1 month storage in its mother liquid (e.g., **2-$Co_{1.64}Ni_{2.36}$-PF_6**, cf. Figure S6d and Table S3 for crystallographic data and Figures S45d and S53b for analytical purity). In contrast, such a dissociation of the bridging acetate group was not observed for **2-μ-OAc-Co_xNi_{4-x}-Cl** and **-NO_3**, even when stored in saturated solutions of NaCl or $NaNO_3$.

Counteranion Concentration and Type 1 Co/Ni Cubanes. Interestingly, higher concentrations of these specific counteranions (Cl^- and NO_3^-) enable the transformation of **2-μ-OAc-Co_xNi_{4-x}** ($Ni(OAc)_2$:$Co(OAc)_2 \leq$ 1:3) into new mixed **type 1** cubanes (Scheme 1 and Figures S2, S57−S62); note that $NaNO_3$ still gave rise to a mixture of **2-μ-OAc-Co_xNi_{4-x}-NO_3** and **1-Co_xNi_{4-x}-3OAc-NO_3** (Scheme 1 and Figure S58). Phase pure **1-Co_xNi_{4-x}-4Cl** cubanes can be accessed with higher NaCl amounts (≥6.25 equiv), such as **1-$Co_{3.31}Ni_{0.69}$-4Cl** emerging from $Co(OAc)_2/Ni(OAc)_2$ = 0.6 mmol/0.2 mmol (ICP elemental analyses, cf. also Scheme 1, Figures 5 and S52b). In contrast, addition of only 0.125−0.5 equiv $NaPF_6$ to the same precursor mixture immediately provided phase pure **1-$Co_{3.28}Ni_{0.72}$-3OAc-PF_6** (ICP elemental analyses, Scheme 1, Figures S44a and S52c).

Given that the counteranion concentration is the salient difference between all these analogous synthetic pathways, we note that a remarkable extent of anion-induced *structure control in solution* is at work here that *differs notably from a mere cocrystallization effect*.

The selective influence of the *counteranion type* in solution is furthermore illustrated in Scheme 1 within the given $Ni(OAc)_2$:$Co(OAc)_2$ ratio ranges. An illustrative example is the absence of the above-described retransformation from **type 2** Co/Ni cubanes to **type 1** when applying higher $NaClO_4$, $NaClO_3$, or $NaBF_4$ concentrations (according analyses of crystalline samples and analytical protocols are given in the SI, p. S34−S35, Figures S45 and S53).

Overview. In conclusion, we provide counteranion-directed control over cubanes on three structural levels: (1) differentiation between **types 1**/**2**, (2) access to specific mixed **type 1** and **2** Co/Ni cubane compositions, and (3) adjustment of cubane ligand patterns for both types. This new territory of highly selective functionalities of straightforward inorganic counteranions in the assembly process of transition metal oxo clusters is first covered with mechanistic studies in the following.

Experimental Investigation of Counteranion-Directed $\{Co_4O_4\}$ Cubane Assembly Mechanisms. *Strategy.* Understanding the dynamic hydration behavior of anions in solution remains a fundamental challenge for current analytical and computational research in its own right, as outlined in the Introduction.[42−46] The absence of such detailed insight renders full computational analyses of counteranion-directed cluster assembly processes impossible to date. Likewise, the development of methodologies for their direct in situ monitoring is a research topic on its own.

Therefore, we here designed a set of systematic screening experiments and computational models that sheds light on the basic role of the counteranions in differentiating between **type 1** and **2** cubanes. We started with three basic working hypotheses about the selective formation of cubane types. For the sake of conciseness, we here summarize our main mechanistically relevant results that support our retrosynthetic concept. We refer to the extensive SI for analytical data of the compounds discussed in the following.

1. Hypothesis: Crystal Packing Effects. We first proposed the presence of both **type 1** and **2** cubane cations in solution. Such mixtures would then be driven toward selective crystallization of the optimal packing motif by the respective counteranion. However, the formation of pure **1-4OAc** (60% yield on the basis of dpk, Figure 3a) from the standard synthetic protocol in the absence of further counteranions does not support this assumption. Furthermore, the synthetic routes to $\{Co_4O_4\}$ (Scheme 1) and mixed Co/Ni cubanes (cf. Co:Ni

DOI: 10.1021/jacs.9b01356
J. Am. Chem. Soc. XXXX, XXX, XXX−XXX

ratios of 3:1 in Scheme 1) clearly provide counteranion-dependent access to both **type 1** and **2** cubanes. This underscores their active structure-directing role in solution that goes beyond mere crystal packing effects. As mentioned in the structural discussion above and shown in the SI, most counteranions occupy generic positions in the analogous cubane crystal structure types, which does not point to any selective solid state templating effects (cf. Figures S3–S10).

2. Hypothesis: ClO_4^- and Metal Precursors. Both previous works[70,71] and our own UV–vis spectroscopy studies (Figures 6a and S64) indicate an equilibrium between free Co ions

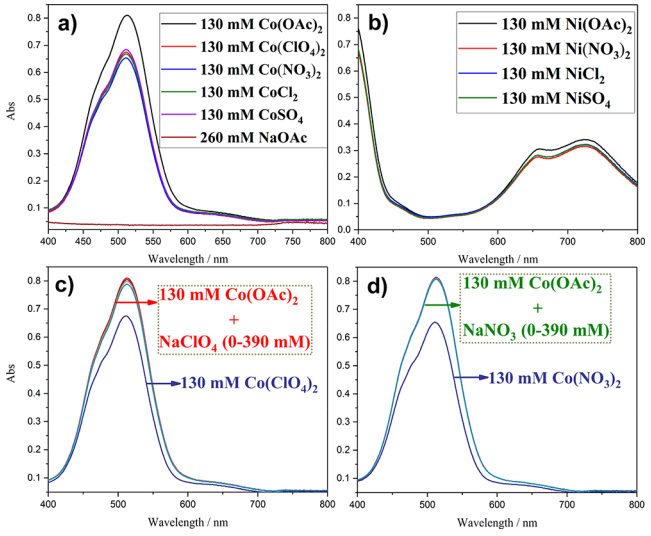

Figure 6. UV–vis spectra of 130 mM $Co(OAc)_2$ (aq.) (a) and $Ni(OAc)_2$ (aq.) (b) vs other cobalt and nickel salts (aq.). UV–vis spectra of pure 130 mM $Co(OAc)_2$ (aq.) and after addition of different amounts of $NaClO_4$ (c) and $NaNO_3$ (d).

$[Co(H_2O)_6]^{2+}$ (abbreviated as $[Co]^{2+}$ in the following) and $[Co(H_2O)_5(OAc)]^+$ (short: $[Co(OAc)]^+$) in the dissociation of the precursor material $Co(OAc)_2$ (aq.). A formal retrosynthetic analysis of both cubane types shows that **1-4OAc** contains only the $[Co(OAc)]^+$ building block, while **type 2** is formally constituted of both $[Co]^{2+}$ and $[Co(OAc)]^+$ moieties (Figure 7a). As **type 2** $\{Co_4O_4\}$ cubanes could selectively be obtained in the presence of $NaClO_4$ (Scheme 1), one might argue that higher ClO_4^- concentrations could facilitate the release of $[Co]^{2+}$ from $Co(OAc)_2$ (aq.) toward the concentrations required for **type 2** cubane assembly (Figure S63b).

However, the UV–vis spectrum of $Co(OAc)_2$ + 3 equiv $NaClO_4$ (aq.) is almost identical to that of pure $Co(OAc)_2$ solutions and differs considerably from $Co(ClO_4)_2$ (aq.) (Figure 6c). As a consequence, the direct interaction between ClO_4^- and the $Co(OAc)_2$ precursor is unlikely to promote **type 2** cubane formation.

3. Hypothesis: Retrosynthetic Approach. Therefore, we proposed in our main working hypothesis the assembly of **type 1** and **2** cubanes from their retrosynthetic building blocks $[Co_2(dpy\text{-}C\{OH\}O)_2(OAc)_2(H_2O)_2]$ and $[Co_2(dpy\text{-}C\{OH\}O)_2(H_2O)_4]^{2+}$ via different anion-dependent pathways. Both building blocks are shown in Figure 7b and c and are abbreviated as $[Co_2(dpy\text{-}C\{OH\}O)_2(OAc)_2]$ and $[Co_2(dpy\text{-}C\{OH\}O)_2]^{2+}$ in the following. We further postulate that the intermediate $[Co_2(dpy\text{-}C\{OH\}O)_2(OAc)_2]$ is formed first

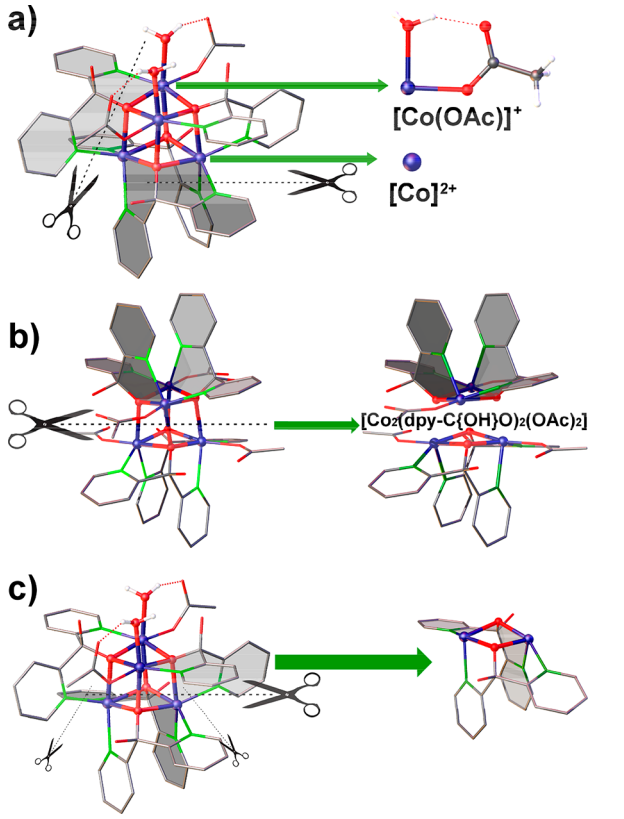

Figure 7. Retrosynthetic analyses of the coordination reaction (a) and of **type 1** and **2** (b,c) cubanes based on the respective dimeric building block.

upon addition of dpk into $Co(OAc)_2$ (aq.) in any given synthetic route (Figure 8), which is in line with previous synthetic studies.[72]

3.1. Different Pathway Options to Types 1 and 2 Cubanes. In the absence of additional counteranions, $[Co_2(dpy\text{-}C\{OH\}O)_2(OAc)_2]$ can either combine with each other or react with $[Co(OAc)]^+$ and dpy-C{OH}O$^-$ ligands to form the fully acetate-substituted **1-4OAc** cubane (Figure 8a,b). **1-3OAc**, **1-2OAc**, or **1-4Cl** cubanes can then be formed through addition of structure-directing ClO_3^-, BF_4^-, PF_6^-, NO_3^-, and Cl^- anions. We obtained an indication for an anion-driven OAc^- ligand dissociation from **type 1** cubanes through the observed transition from pure **1-3OAc-BF_4** products over a mixture with their **1-2OAc** analogues to pure **1-2OAc-2BF_4** upon increased counteranion amounts (cf. Scheme 1, upper entries). Moreover, we *did not* observe conversion of **1-2OAc-ClO_4** into its **type 2**-edge-site analogue with excess ClO_4^-, despite its $[Co_2(dpy\text{-}C\{OH\}O)_2(H_2O)_2]$ building block. This is additional support for independent assembly pathways of **type 1** and **2** cubanes. Figure 8 presents three plausible pathways that are further discussed in the following.

3.2. Selectivity of ClO_4^- for Type 2 Cubanes. As outlined for hypothesis 2 above, ClO_4^- does not significantly interfere with the $[Co(OAc)]^+/[Co]^{2+}$ equilibrium. Nevertheless, we have strong experimental indications that ClO_4^- can indeed selectively induce the dissociation of acetate ligands from cubanes. For example, only >0.31 equiv ClO_4^- are sufficient to convert bridged **2-μ-OAc-Co_xNi_{4-x}** into its edge-site **type 2** analogue, while far higher concentrations (5 and/or 6.25 equiv) of ClO_3^- and BF_4^- are required to induce this conversion (Scheme 1). Further clear evidence for such

DOI: 10.1021/jacs.9b01356
J. Am. Chem. Soc. XXXX, XXX, XXX–XXX

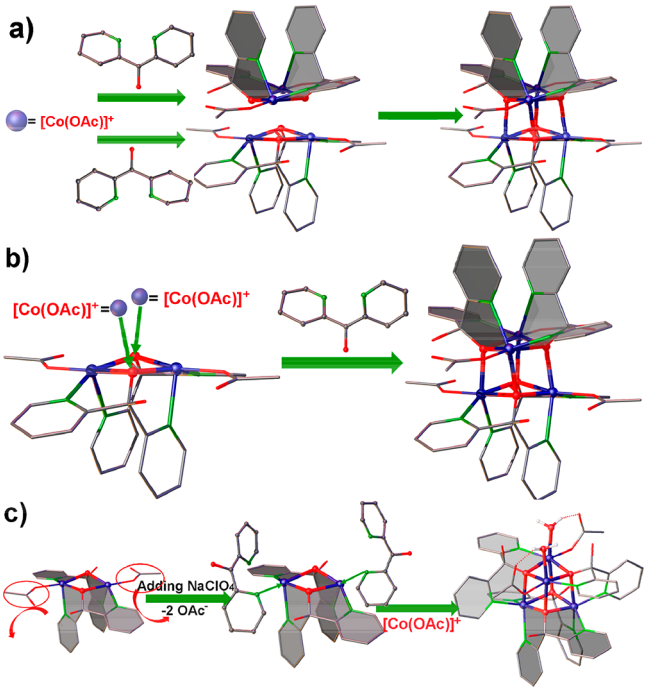

Figure 8. Possible assembly pathways of **type 1** (a,b) and **type 2** cubanes (c). Aqua ligands on the dimeric intermediates are omitted for clarity.

ClO_4^- induced acetate ligand dissociation is the facile transformation of **1-3OAc-BF$_4$** into phase pure **1-2OAc-2ClO$_4$** within a few hours in the presence of a moderate 10-fold molar excess of ClO_4^-. In drastic contrast, obtaining pure **1-2OAc** through BF_4^- addition requires a massive 700-fold molar excess (cf. SI for experimental details and Figures 9 and S34 for analytical characterizations).

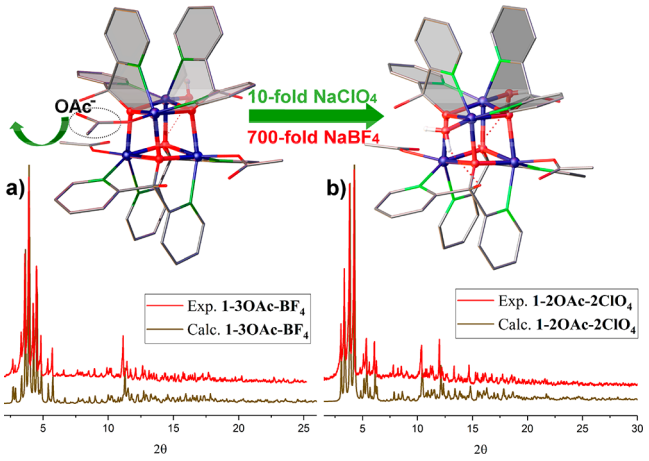

Figure 9. PXRD patterns of cubane products supporting the pathway of **1-2OAc** formation via ClO_4^- induced dissociation of acetate ligands from **1-3OAc**.

With clear indications for this role of ClO_4^- at hand, we conclude that it can also facilitate acetate removal from $[Co_2(dpy\text{-}C\{OH\}O)_2(OAc)_2(H_2O)_2]$ to form the building block $[Co_2(dpy\text{-}C\{OH\}O)_2(H_2O)_4]^{2+}$ (Figure 8c). Given that almost all perchlorate-assisted routes afford **type 2** cubanes (Scheme 1), we conclude that they are plausibly formed via **pathway c** of Figure 8.

Consequently, **type 1** cubanes are more likely formed via the **pathways a** and **b** shown in Figure 8.

3.3. Evidence for the Building Block $[Co_2(dpy\text{-}C\{OH\}O)_2(OAc)_2(H_2O)_2]$. To further support these proposed formation pathways, we first attempted to isolate the key dimer $[Co_2(dpy\text{-}C\{OH\}O)_2(OAc)_2(H_2O)_2]$ from ethanol while adding $LiOH{\cdot}H_2O$, following the reported procedure for its Zn-analogue $[Zn_2(dpy\text{-}C\{OMe\}O)_2Cl_2]$.[73] Although this route remained unsuccessful, we nevertheless obtained a defect cubane from asymmetric assembly of two dimeric $[Co_2(dpy\text{-}C\{OH\}O)_2(OAc)_2]$ moieties. Interestingly, this defect cubane was converted into **1-4OAc** after 2 weeks of storage in its mother liquid (Figure S65, cf. Table S8 for crystallographic data and Figure S25 for analytical characterization). This result supports the crucial role of the building block $[Co_2(dpy\text{-}C\{OH\}O)_2(OAc)_2(H_2O)_2]$ in cubane assembly.

One reason for the difficulties in isolating this key building block may arise from the high reactivity of its η^2-oxygen center toward $[Co(OAc)]^+$ or toward the Co site of another $[Co_2(dpy\text{-}C\{OH\}O)_2(OAc)_2(H_2O)_2]$ moiety. To check this assumption, we synthesized the phenyl-modified dpk ligand 1,1-bis(2-pyridyl)phenylmethanol where the bulky substituent might prevent the dimerization of the intermediates. This precursor indeed afforded the expected dimer $[Co_2(dpy\text{-}C\{Ph\}O)_2(OAc)_2]$ as crucial support for the proposed pathways via dimeric Co species (Figure S11b and Table S8).

3.4. Key Experimental Evidence for Type 1 and 2 Formation Pathways. Next, we used $Co(NO_3)_2$ as acetate-free Co^{2+} source to further differentiate between **pathways a**–**c** through excluding any acetate coordination to the dimeric intermediate $[Co_2(dpy\text{-}C\{OH\}O)_2(H_2O)_4]^{2+}$.

As another strong indication for the assembly of **type 2** cubanes via **pathway c**, the new **type 2** cubane $[Co_4(dpy\text{-}C\{OH\}O)_4(H_2O)_4](NO_3)_4$ (**2-(*gem*-aqua)-Co$_4$-NO$_3$**) with a *gem*-aqua $\{Co_2(H_2O)_4\}$ edge-site was formed as expected (Figures 10a, cf. Figure S8a and Table S6 for crystallographic data).

Surprisingly, the new compound $[Co_5(dpy\text{-}C\{OH\}O)_5(dpy\text{-}C\{O\}_2](NO_3)_3$ (**2-[Co$_5$]-NO$_3$**) with a $[Co(dpy\text{-}C\{OH\}O)_2]$ moiety coordinated to the edge-site cocrystallized with **2-(*gem*-aqua)-Co$_4$-NO$_3$** (Figure S12 and Table S7). Pure **2-(*gem*-aqua)-Co$_4$-NO$_3$** can be obtained through applying a starting ratio of $Co(NO_3)_2$/dpk = 1.5 instead of 1 (Figures S45 and S56).

We then analyzed the influence of acetate anions on the synthetic pathway through varying the initial $[Co]^{2+}/[Co(OAc)]^+$ ratios. First, a $[Co]^{2+}/[Co(OAc)]^+$ ratio >1 (i.e., ≤0.2 mmol NaOAc/0.4 mmol $Co(NO_3)_2$ (aq.)) gave rise to **2-Co$_4$-NO$_3$**, indicating that the dpk ligand reacts more readily with free $[Co^{2+}]$ according to **pathway c** (Figures 10a, cf. Figure S10c and Table S7 for crystallographic data and Figures S35 and S45 for analytical characterizations). Formation of **2-Co$_4$-NO$_3$** under these conditions also demonstrates that the presence of ClO_4^- is convenient, but not an absolutely necessary criterion for **type 2** cubane formation.

Second, $[Co]^{2+}/[Co(OAc)]^+$ ratios <1 trigger a change to **1-3OAc-NO$_3$**, which strongly suggests that **pathways a** or **b** prevail when $[Co(OAc)]^+$ is present as major species (cf. Figure S64 for predominance of $[Co(OAc)]^+$ in analogous conditions, Figure S5b and Table S2 for crystallographic data and Figures S38 and S43b for analytical characterizations). These conclusions were backed up with analogous results of

DOI: 10.1021/jacs.9b01356
J. Am. Chem. Soc. XXXX, XXX, XXX−XXX

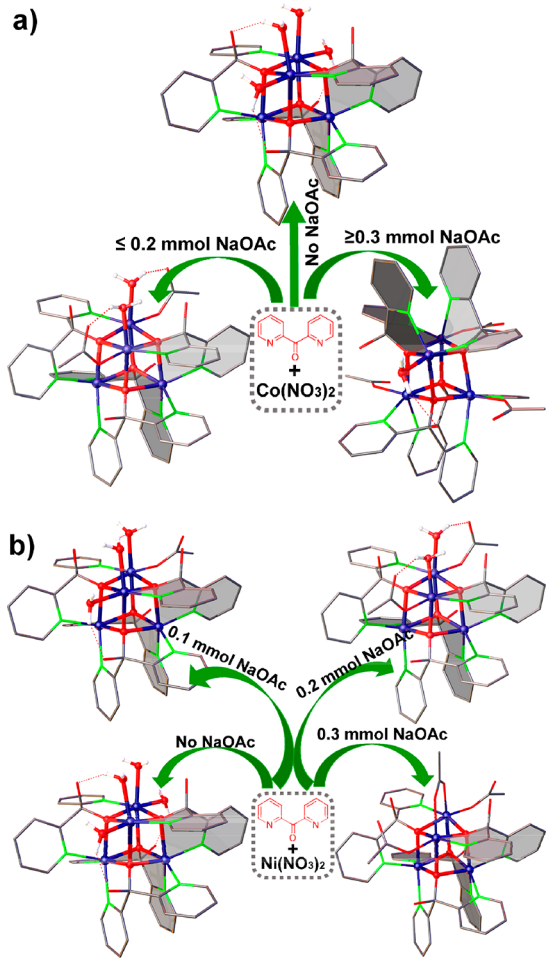

Figure 10. Representations of $\{Co_4O_4\}$ (a) and $\{Ni_4O_4\}$ (b) cubane syntheses through addition of 0.4 mmol dpk (aq.) into an aqueous solution of 0.4 mmol $M(NO_3)_2$ in the presence of increasing amounts of NaOAc.

the same synthetic screenings in the presence of chlorate and tetrafluoroborate counteranions instead of nitrate (cf. Figure S5, S10 and Tables S2 and S7 for the crystallographic data and Figures S36, S37, and S45 for analytical characterizations).

Conclusions for {Co$_4$O$_4$} Cubane Formation. Collected experimental evidence from the first part of our systematic mechanistic study clearly supports (a) the active role of counteranions in the cluster assembly process, (b) the key role of the $[Co_2(dpy\text{-}C\{OH\}O)_2(OAc)_2]$ and $[Co_2(dpy\text{-}C\{OH\}O)_2]^{2+}$ building blocks, and (c) their participation in **pathways a**/**b** and **c** giving rise to **type 1** and **2** cubanes, respectively.

Computational Studies. Starting from our comprehensive experimental support for the assembly of **type 1** and **2** cubanes via their respective dimeric moieties $[Co_2(dpy\text{-}C\{OH\}O)_2(OAc)_2(H_2O)_2]$ and $[Co_2(dpy\text{-}C\{OH\}O)_2(H_2O)_4]^{2+}$, we applied density functional theory (DFT) computations (cf. SI for details) to further corroborate our retrosynthetic hypotheses. First, the calculated thermodynamic stabilities of various monomeric and dimeric building blocks were compared and then combined with the experimental observations to identify the most plausible assembly pathways. Due to the similar coordination behavior of Co^{2+} and Ni^{2+} ions toward the dpk ligand, calculations were representatively performed for the cobalt compounds in the following. The results can presumably be applied to the assembly of $\{Ni_4O_4\}$ and $\{Co_xNi_{4-x}O_4\}$ cubanes as well.

First, the optimized structures of four possible dimer types with acetate-coordinated Co centers, namely, $[Co_2(dpy\text{-}C\{OH\}O)_2(\mu\text{-}OAc)_2]$ (**D1**), $[Co_2(dpy\text{-}C\{OH\}O)_2(OAc)_2]$ (**D2**), $[Co_2(dpy\text{-}C\{OH\}O)_2(OAc)_4]^{2-}$(**D3**), and $[Co_2(dpy\text{-}C\{OH\}O)_2(OAc)_2(H_2O)_2]$ (**D4**) (Figure 11) were generated.

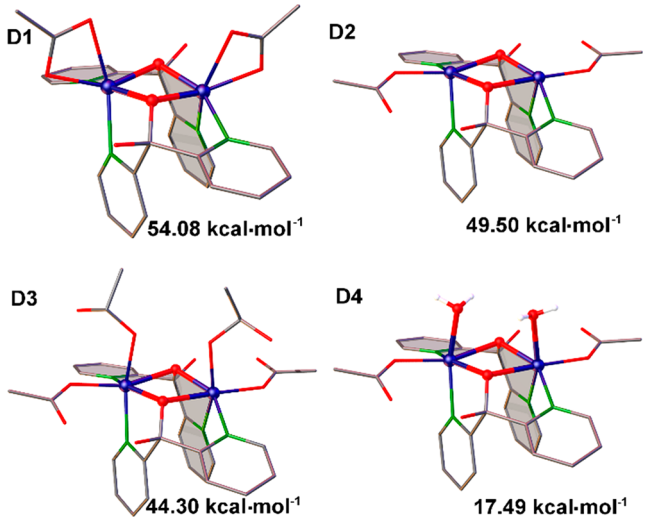

Figure 11. Co dimeric building blocks subjected to computational studies.

The relative energy comparison of these most probable dimers **D1**-**4** revealed that **D4** is indeed the thermodynamically most stable species (Figure 11). This result corresponds well with its crucial role that emerged from our experimental probing of the cubane assembly pathways. The computed reaction energy suggests that **1-4OAc** indeed results from direct head-to-head combination of two **D4** dimers via **pathway a** (Figures 8a and S68a), where the dpk ligand adopts a tridentate coordination mode. Furthermore, the reaction energies for various assembly pathways of **1-4OAc** via different $[Co(dpy\text{-}C\{OH\}O)(OAc)_n(H_2O)_m]^{2-n}$ monomers were calculated (Figure S69 and Table S20) and found to be thermodynamically less feasible than **pathway a**. All in all, DFT calculations fully support the experimentally postulated formation **pathway a** of **1-4OAc** (Figures 8a and S68a).

On the basis of the above energy comparisons (summarized in Table S20), the most stable Co monomer was found to be $[Co(dpy\text{-}C\{OH\}O)(OAc)(H_2O)_3]$ arising from $[Co(H_2O)_5(\mu_1\text{-}OAc)]^+$ coordinating with one N and O^- of dpy-$C\{OH\}O^-$ in *cis*- and *trans*-position to the OAc^- ligand (**M12**, Figure S69). Assuming that increasing the ionic strength of the reaction solution, e.g., through perchlorate addition, encourages **M12** formation, these monomers can further react with **D4** via acetate ligand dissociation to afford **2-Co$_4$-ClO$_4$** (Figure S68b). This plausible route corresponds well with the experimentally postulated **pathway c** toward **type 2** cubane assembly.

Formation Pathways of Ni-Containing Cubanes. *Influence of Ni^{2+} and OAc^- on Type 2 Cubane Assembly.* With this insight on $\{Co_4O_4\}$ cubanes at hand, we reasonably assumed that **type 2** $\{Ni_4O_4\}$ cubanes assemble through **pathway c**. This agrees well with the observed predominance of $[Ni(H_2O)_6]^{2+}$ (abbreviated as $[Ni]^{2+}$) when comparing the UV−vis spectrum of $Ni(OAc)_2$ (aq.) to other Ni^{2+} salts of

DOI: 10.1021/jacs.9b01356
J. Am. Chem. Soc. XXXX, XXX, XXX−XXX

strong acids (Figure 6b), as well as with previous studies.[74] $[Ni]^{2+}$ and dpk are very likely to form the main intermediate $[Ni_2(dpy\text{-}C\{OH\}O)_2(H_2O)_4]^{2+}$ with a strong preference for **type 2** cubane formation (Scheme 1). Indeed, reference reactions in acetate-free media with $Ni(NO_3)_2$ as $[Ni]^{2+}$ source afforded the expected *gem*-aqua $\{Ni_4O_4\}$ cubane $[Ni_4(dpy\text{-}C\{OH\}O)_4(H_2O)_4](NO_3)_4$, **2(*gem*-aqua)-Ni$_4$-NO$_3$** (Figure 10b, cf. Figure S8b and Table S6 for crystallographic data and Figures S45 and S56 for analytical characterization).

Moreover, the $\{Ni_4O_4\}$ cubane types obtained from increasing initial NaOAc contents support **pathway c**. Interestingly, the addition of 0.25 equiv NaOAc results in a new **type 2** compound, namely, $[Ni_4(dpy\text{-}C\{OH\}O)_4(OAc)(H_2O)_3](NO_3)_3$ (**2(half-*gem*-aqua)-Ni$_4$-NO$_3$**), where one aqua ligand parallel to the {NiONiO} plane is replaced by OAc^- (Figures 10b, cf. S9 and Table S6 for crystallographic data and Figure S56 for analytical characterizations). This indicates a different substitutional behavior of the *gem*-aqua ligands on the $\{Ni_2(H_2O)_4\}$ edge-site toward stronger donor ligands. Finally, this directed ligand assembly of $\{Ni_4O_4\}$ cubanes as a function of increasing initial OAc^- content was supported through the formation of **2-Ni$_4$-NO$_3$** and **2-μ-OAc-Ni$_4$-NO$_3$** with 0.5 equiv and ≥0.75 equiv, respectively (Figure 10b, cf. Figure S7c, Table S5, and Table S6 for crystallographic data and Figures S45, S53, and S55 for analytical characterizations).

Interplay of Ni^{2+} and Co^{2+} in Cubane Formation. Furthermore, the key role of free $[M]^{2+}$ species in **type 2** cubane formation via intermediate $[Co_2(dpy\text{-}C\{OH\}O)_2(H_2O)_4]^{2+}$ became evident from the strongly selective formation of mixed **type 2** cubanes even in the presence of low initial Ni contents (0.6 mmol $Co(OAc)_2$ + 0.2 mmol $Ni(OAc)_2$, Scheme 1). In light of the above, we assume that the dpk ligand first reacts with the predominant $[Ni]^{2+}$ species to the corresponding Ni-rich $[M_2(dpy\text{-}C\{OH\}O)_2(H_2O)_4]^{2+}$ intermediate to provide **type 2** $\{Co_xNi_{4-x}O_4\}$ products in the presence of ClO_3^-, BF_4^-, and PF_6^- via **pathway c**. Indeed, the actual ratios of Co:Ni in all obtained **2-Co$_x$Ni$_{4-x}$-ClO$_3$**, **-BF$_4$**, and **-PF$_6$** always fall below the respective initial ratios (Table S17). The above-mentioned (section 3.2.) directing effect of ClO_4^- on cubane fragments and acetate anions apparently releases higher $[Co]^{2+}$ concentrations for **type 2** cubane formation. This agrees with the observed higher Co content of as-synthesized **2-Co$_x$Ni$_{4-x}$-ClO$_4$** compared to the **2-Co$_x$Ni$_{4-x}$-ClO$_3$**, **-BF$_4$**, and **-PF$_6$** products obtained from identical Co:Ni starting ratios (ICP-MS measurements in Table S17).

Consequently, relatively low amounts of free $[M]^{2+}$ should lead to insufficient concentrations of the **type 2** building-block $[M(dpy\text{-}C\{OH\}O)_2(H_2O)_4]^{2+}$ in the presence of other counteranions than ClO_4^-. Indeed, we observed that BF_4^- and ClO_3^- addition led to (partial) **type 1** cubane formation under analogous conditions, such as a mixture of **1-Co$_x$Ni$_{4-x}$-3OAc-BF$_4$** and **2-μ-OAc-Co$_x$Ni$_{4-x}$-BF$_4$** obtained from 0.7 mmol $Co(OAc)_2$ + 0.1 mmol $Ni(OAc)_2$ with 3 mmol $NaBF_4$ (Figures S66a and S67). Similarly, **1-Co$_x$Ni$_{4-x}$-3OAc-ClO$_3$** was synthesized from 0.7 mmol $Co(OAc)_2$ + 0.1 mmol $Ni(OAc)_2$ and 3 mmol $NaClO_3$. Additionally, this product further expanded the spectrum of **type 1** $\{Co_xNi_{4-x}O_4\}$ cubanes (Figure S66b and S67).

Mixed Co/Ni Pathways. In summary, mixed **type 2** cubanes can generally be accessed from precursors containing ca. ≥25 mol % Ni^{2+} cations due to their strong preference for the experimentally supported **pathway c**, even in the absence of further structure-directing perchlorate anions.

Visible-Light-Driven Water Oxidation Studies. We furthermore carried out visible-light-driven water oxidation studies to compare the influence of structural features on the catalytic activity of specific cubane types. To this end, we selected a set of non-edge-site, $\{H_2O\text{-}Co_2(OR)_2\text{-}OH_2\}$ edge-site, *gem*-aqua $\{Co(OH_2)_4\}$ edge-site, and edge-site-blocked catalysts, namely, **1-3OAc-ClO$_4$**, **2-Co$_4$-ClO$_4$**, **2(*gem*-aqua)-Co$_4$-NO$_3$**, and **2-[Co$_5$]-NO$_3$**, respectively.

These cubanes were tested at pH 8.5 in 80 mM borate buffer solution containing 1 mM $[Ru(bpy)_3]Cl_2$ as photosensitizer and 5 mM $Na_2S_2O_8$ as sacrificial electron acceptor (Figure 12 and Table S18 as well as experimental part of the SI). **2-Co$_4$-ClO$_4$** with the edge-site motif is more active than the non-edge-site cubane **1-3OAc-ClO$_4$**, which relates well with our previous studies.[56] Furthermore, **2(*gem*-aqua)-Co$_4$-NO$_3$** exhibited the best catalytic performance with a turnover number (TON) of 20.8, a turnover frequency (TOF) of 0.27 s^{-1}, and an O_2 evolution yield of 83.0%. This activity is rather high compared to previous works on analogous cubane WOCs,[54,55,75−77] indicating that the aqua ligand-enriched *gem*-aqua is likely to promote the oxygen evolution activity. Along these lines, **2-[Co$_5$]-NO$_3$** showed the lowest activity with a TON of 11.5, a TOF of 0.10, and an O_2 evolution yield of 46%. This result further indicates that the accessibility of the edge-site is indeed relevant for the catalytic activities of the cubane catalyst series. Our systematic synthetic approach now provides convenient access to such tuned cubanes for forthcoming detailed structure−activity studies in their own right.

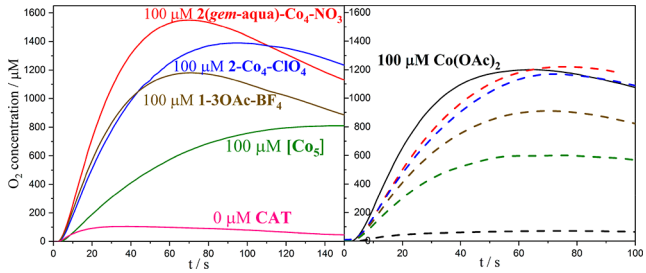

Figure 12. Clark electrode kinetics of visible-light-driven water oxidation of the pristine catalysts (solid curves, left) and of their respective filtered postcatalytic reaction solutions (dashed curves, right; conditions: 470 nm LED, 1 mM $[Ru(bpy)_3]Cl_2$, 5 mM $Na_2S_2O_8$, pH 8.5 80 mM borate buffer). The pH value was readjusted 8.5 by adding solid $Na_2B_4O_7{\cdot}10H_2O$ after each reaction.

Cubane catalyst stability was studied with a sequence of filtration and activity tests of the recycled postcatalytic reaction solution.[56,78] All cubane catalysts retained most of their catalytic activities during the recycling runs. In contrast, the reference tests with $Co(OAc)_2$ mimicking the behavior of in situ formed CoO_x particles showed no activity in the recycling run (Figure 12). This provided strong evidence that all the cubanes remained in molecular states after the first catalytic run.

CONCLUSIONS

We introduce an unprecedented controlled access to a large family of $\{M_4O_4\}$ (M = Co, Ni, and Co/Ni) bioinspired cubane photocatalysts. A toolbox of straightforward inorganic

DOI: 10.1021/jacs.9b01356
J. Am. Chem. Soc. XXXX, XXX, XXX−XXX

counteranions directs the assembly of the di(2-pyridyl) ketone (dpk) ligand and $M(OAc)_2$ precursors in aqueous solution into clearly accessible cubane types:

Type 2 $\{Co_4O_4\}$ cubanes with the characteristic $\{H_2O\text{-}Co_2(OR)_2\text{-}OH_2\}$ edge-site motif are selectively obtained with perchlorate anions. In contrast, a wide range of counteranions ($\leq$0.5 equiv of ClO_4^-, and ClO_3^-, NO_3^-, BF_4^-, Cl^-, PF_6^-) provide access to **type 1** Co-cubanes with adjustable ligand patterns. **Type 2** edge-site $\{Ni_4O_4\}$ cubanes are formed with >0.3 equiv ClO_4^-, while all other tested counteranions provide **2-μ-OAc-Ni$_4$**. The **2-Co$_x$Ni$_{4-x}$** and **2-μ-OAc-Co$_x$Ni$_{4-x}$** cubanes can be tailored via counteranion controlled assembly of mixed precursors. Furthermore, the homogeneous visible-light-driven water oxidation activity of **type 1** and **type 2** $\{Co_4O_4\}$ cubanes with increasingly accessible edge-site regions was compared.

Systematic screenings provided cumulative experimental evidence for **type 2** and **1** $\{Co_4O_4\}$ cubane assembly via two main building blocks, namely, $[Co_2(dpy\text{-}C\{OH\}O)_2(H_2O)_4]^{2+}$ and $[Co_2(dpy\text{-}C\{OH\}O)_2(OAc)_2(H_2O)_2]$. DFT calculations confirmed that $[Co_2(dpy\text{-}C\{OH\}O)_2(OAc)_2(H_2O)_2]$ is indeed thermodynamically most stable of all investigated dimer types in solution. Computed reaction energies agree with the experimentally supported formation pathway of **type 1** cubane **1-4OAc** through a head-to-head combination of these dimers. Furthermore, DFT results indicate that **type 2** cubanes arise from the reaction of the $[Co_2(dpy\text{-}C\{OH\}O)_2(OAc)_2(H_2O)_2]$ dimer with the most stable $[Co(dpy\text{-}C\{OH\}O)(OAc)\text{-}(H_2O)_3]$ monomer that is likely to result from higher applied perchlorate strengths. The selective access to **type 2** $\{Ni_4O_4\}$ and **type 2** mixed $\{(Co/Ni)_4O_4\}$ cubanes proceeds via combinations of according Ni-dimers with predominant $[Ni^{2+}]$ species through analogous assembly processes.

We reveal for the first time the high potential of convenient inorganic counteranions as structure-directing agents for oxo cluster assembly in solution. The formation pathways leading to an arsenal of transition metal cubanes were tracked with an effective combination of mechanistic screening going hand in hand with DFT calculations. Our extensive data set offers an excellent platform the for forthcoming machine learning explorations of the full parameter space in coordination chemistry. We here first pave the way to facile, predictive, and mechanistically driven design concepts for the strategic construction of functional transition metal complexes.

■ ASSOCIATED CONTENT

Supporting Information

The Supporting Information is available free of charge on the ACS Publications website at DOI: 10.1021/jacs.9b01356.

Detailed synthetic and catalytic protocols, stability tests, analytical investigations, and computational methods and results (PDF)

Crystal data (also deposited as CCDC 1891281-1891291, 1891332-1891335, 1891347-1891350, 1891352-1891357, 1891359-1891361, and 1891379-1891384) (CIF)

■ AUTHOR INFORMATION

Corresponding Author

*greta.patzke@chem.uzh.ch

ORCID

Fangyuan Song: 0000-0002-9563-1926

Karrar Al-Ameed: 0000-0002-8333-3868

Mauro Schilling: 0000-0002-9394-4726

Thomas Fox: 0000-0002-7572-8210

Sandra Luber: 0000-0002-6203-9379

Greta R. Patzke: 0000-0003-4616-7183

Notes

The authors declare no competing financial interest.

■ ACKNOWLEDGMENTS

This work has been supported by the University of Zurich, the University Research Priority Program (URPP) for Solar Light to Chemical Energy Conversion (LightChEC), and by the Swiss National Science Foundation (Sinergia Grant No. CRSII2_160801/1). S. Luber thanks the Swiss National Science Foundation (Grant No. PP00P2_170667) for financial support. K. Al-Ameed thanks the Swiss Government Excellence Scholarships for Foreign Scholars and Artists for financial support. We thank Prof. Dr. Anthony Linden and Dr. Olivier Blacque (Department of Chemistry, University of Zurich) for helpful crystallographic discussions. We are grateful to PD Dr. Laurent Bigler (Department of Chemistry, University of Zurich) for support and discussions concerning HR-ESI-MS measurements.

■ REFERENCES

(1) Ryan, K.; Lengyel, J.; Shatruk, M. Crystal Structure Prediction via Deep Learning. *J. Am. Chem. Soc.* **2018**, *140*, 10158−10168.

(2) Coley, C. W.; Green, W. H.; Jensen, K. F. Machine Learning in Computer-Aided Synthesis Planning. *Acc. Chem. Res.* **2018**, *51*, 1281−1289.

(3) Kim, E.; Huang, K.; Jegelka, S.; Olivetti, E. Virtual screening of inorganic materials synthesis parameters with deep learning. *NPJ Comput. Mater.* **2017**, *3*, 1120.

(4) Bijelic, A.; Aureliano, M.; Rompel, A. Polyoxometalates as Potential Next-Generation Metallodrugs in the Combat Against Cancer. *Angew. Chem., Int. Ed.* **2019**, *57*, 2−22.

(5) Genovese, M.; Lian, K. Polyoxometalate modified inorganic−organic nanocomposite materials for energy storage applications: A review. *Curr. Opin. Solid State Mater. Sci.* **2015**, *19*, 126−137.

(6) Xu, G.; Wang, Z.; Ling, R.; Zhou, J.; Chen, X.-D.; Holm, R. H. Ligand metathesis as rational strategy for the synthesis of cubane-type heteroleptic iron-sulfur clusters relevant to the FeMo cofactor. *Proc. Natl. Acad. Sci. U. S. A.* **2018**, *115*, 5089−5092.

(7) Luo, Z.; Zhou, M.; Wang, X. Cobalt-based cubane molecular co-catalysts for photocatalytic water oxidation by polymeric carbon nitrides. *Appl. Catal., B* **2018**, *238*, 664−671.

(8) Schwarz, B.; Forster, J.; Goetz, M. K.; Yücel, D.; Berger, C.; Jacob, T.; Streb, C. Visible-Light-Driven Water Oxidation by a Molecular Manganese Vanadium Oxide Cluster. *Angew. Chem., Int. Ed.* **2016**, *55*, 6329−6333.

(9) Maayan, G.; Gluz, N.; Christou, G. A Bioinspired Soluble Manganese Cluster as a Water Oxidation Electrocatalyst with Low Overpotential. *Nat. Catal.* **2018**, *1*, 48−54.

(10) Han, X.-B.; Li, Y.-G.; Zhang, Z.-M.; Tan, H.-Q.; Lu, Y.; Wang, E.-B. Polyoxometalate-based nickel clusters as visible light-driven water oxidation catalysts. *J. Am. Chem. Soc.* **2015**, *137*, 5486−5493.

(11) Han, X.-B.; Zhang, Z.-M.; Zhang, T.; Li, Y.-G.; Lin, W.; You, W.; Su, Z.-M.; Wang, E.-B. Polyoxometalate-based cobalt-phosphate molecular catalysts for visible light-driven water oxidation. *J. Am. Chem. Soc.* **2014**, *136*, 5359−5366.

(12) Lant, H. M. C.; Michaelos, T. K.; Sharninghausen, L. S.; Mercado, B. Q.; Crabtree, R. H.; Brudvig, G. W. N, N, O Pincer Ligand with a Deprotonatable Site that Promotes Redox-Leveling, High Mn Oxidation States, and a Mn2O2 Dimer Competent for Catalytic Oxygen Evolution. *Eur. J. Inorg. Chem.* **2019**, *2019*, 2115−2123.

DOI: 10.1021/jacs.9b01356
J. Am. Chem. Soc. XXXX, XXX, XXX−XXX

(13) Misra, A.; Franco Castillo, I.; Müller, D. P.; González, C.; Eyssautier-Chuine, S.; Ziegler, A.; La Fuente, J. M. de; Mitchell, S. G.; Streb, C. Polyoxometalate-Ionic Liquids (POM-ILs) as Anticorrosion and Antibacterial Coatings for Natural Stones. *Angew. Chem., Int. Ed.* **2018**, *57*, 14926−14931.
(14) Zhang, Y.; Zhang, J.-J.; Jia, A.-Q.; Xin, Z.-F.; Zhang, Q.-F. A Single-Molecule Magnet Tetranuclear [Mn3IIIMnIVO3Cl] Complex with Bis(diisopropylphosphinyl)imide Ligands. *J. Cluster Sci.* **2018**, *29*, 1345−1352.
(15) Lang, Z.-L.; Guan, W.; Wu, Z.-J.; Yan, L.-K.; Su, Z.-M. Building blocks and formation thermodynamics of α-Keggin-type [PW12O40]3- anion. *Comput. Theor. Chem.* **2012**, *999*, 66−73.
(16) Demissie, T. B.; Ruud, K.; Hansen, J. H. DFT as a Powerful Predictive Tool in Photoredox Catalysis: Redox Potentials and Mechanistic Analysis. *Organometallics* **2015**, *34*, 4218−4228.
(17) Tong, Y.-P.; Luo, G.-T.; Zhen, J.; Shen, Y.; Lin, Y.-W. Synthesis, structures, and theoretical investigation of three polyoxomolybdate-based compounds: Self-assembly, fragment analysis, orbital interaction, and formation mechanism. *CrystEngComm* **2015**, *17*, 2629−2635.
(18) Thomas, P.; Chandel, S.; Mallick, A.; Sreejith, S. S.; Ghosh, N.; Roy, S. Studying the Crystallization of Polyoxometalates from Colloidal Softoxometalates. *Cryst. Growth Des.* **2018**, *18*, 4068−4075.
(19) Wong, H.-Y.; Chan, W. T. K.; Law, G.-L. Assembly of Lanthanide(III) Cubanes and Dimers with Single-Molecule Magnetism and Photoluminescence. *Inorg. Chem.* **2018**, *57*, 6893−6902.
(20) Michaelos, T. K.; Shopov, D. Y.; Sinha, S. B.; Sharninghausen, L. S.; Fisher, K. J.; Lant, H. M. C.; Crabtree, R. H.; Brudvig, G. W. A Pyridine Alkoxide Chelate Ligand That Promotes Both Unusually High Oxidation States and Water-Oxidation Catalysis. *Acc. Chem. Res.* **2017**, *50*, 952−959.
(21) Shopov, D. Y.; Sharninghausen, L. S.; Sinha, S. B.; Borowski, J. E.; Mercado, B. Q.; Brudvig, G. W.; Crabtree, R. H. Synthesis of Pyridine-Alkoxide Ligands for Formation of Polynuclear Complexes. *New J. Chem.* **2017**, *41*, 6709−6719.
(22) Libby, E.; Folting, K.; Huffman, C. J.; Huffman, J. C.; Christou, G. Controlled aggregation and deaggregation of a polynuclear oxido-bridged manganese complex: utility to synthesis of the Jahn-Teller effect in high-spin manganese(III). *Inorg. Chem.* **1993**, *32*, 2549−2556.
(23) Nguyen, A. I.; Darago, L. E.; Balcells, D.; Tilley, T. D. Influence of a "Dangling" Co(II) Ion Bound to a MnCo3O4 Oxo Cubane. *J. Am. Chem. Soc.* **2018**, *140*, 9030−9033.
(24) Akhtar, M. N.; Lan, Y.; AlDamen, M. A.; Zheng, Y.-Z.; Anson, C. E.; Powell, A. K. Effect of ligand substitution on the SMM properties of three isostructural families of double-cubane Mn4Ln2 coordination clusters. *Dalton Trans.* **2018**, *47*, 3485−3495.
(25) Modak, R.; Sikdar, Y.; Thuijs, A. E.; Christou, G.; Goswami, S. CoII4, CoII7, and a Series of CoII2LnIII (LnIII = NdIII, SmIII, GdIII, TbIII, DyIII) Coordination Clusters: Search for Single Molecule Magnets. *Inorg. Chem.* **2016**, *55*, 10192−10202.
(26) Christie, L. G.; Asche, S.; Mathieson, J. S.; Vilà-Nadal, L.; Cronin, L. Investigating the Formation of Giant {Pd72}Prop and {Pd84}Gly Macrocycles Using NMR, HPLC, and Mass Spectrometry. *J. Am. Chem. Soc.* **2018**, *140*, 9379−9382.
(27) Tandon, S. S.; Bunge, S. D.; Rakosi, R.; Xu, Z.; Thompson, L. K. Self-assembly of mixed-valence Co(II/III) and Ni(II) clusters: azide-bridged 1D single chain coordination polymers comprised of tetranuclear units, tetranuclear Co(II/III) complexes, ferromagnetically coupled azide-bridged tetranuclear, and hexanuclear Ni(II) complexes: synthesis, structural, and magnetic properties. *Dalton Trans.* **2009**, 6536−6551.
(28) Holló, B.; Rodió, M. V.; Bera, O.; Jovičió, M.; Leovac, V. M.; Tomió, Z. D.; Mészáros Szécsényi, K. Cation- and/or anion-directed reaction routes. Could the desolvation pattern of isostructural coordination compounds be related to their molecular structure? *Struct. Chem.* **2013**, *24*, 2193−2201.
(29) Hu, J.; Zhang, J.; Zhao, J. A.; Hu, L.; Chen, S. Anion-driven Ag(I) coordination architectures: Structural diversity and photoluminescence behaviors. *J. Coord. Chem.* **2016**, *69*, 574−584.
(30) Liu, Y.; Li, J.; Hou, H.; Fan, Y. Subtle role of counteranions in molecular construction: Structures and properties of novel Cu(II) coordination complexes with bis-(1-benzoimidazolymethylene)-(2,5-thiadiazoly)-disulfide. *J. Organomet. Chem.* **2009**, *694*, 2875−2882.
(31) Yang, D.; Zhao, J.; Yang, X.-J.; Wu, B. Anion-coordination-directed self-assemblies. *Org. Chem. Front.* **2018**, *5*, 662−690.
(32) Zhao, J.; Yang, D.; Yang, X.-J.; Wu, B. Anion coordination chemistry: From recognition to supramolecular assembly. *Coord. Chem. Rev.* **2019**, *378*, 415−444.
(33) Müller, M.; Albrecht, M.; Sackmann, J.; Hoffmann, A.; Dierkes, F.; Valkonen, A.; Rissanen, K. CH-anion versus anion-π interactions in the crystal and in solution of pentafluorobenzyl phosphonium salts. *Dalton Trans.* **2010**, *39*, 11329−11334.
(34) Das, A.; Choudhury, S. R.; Estarellas, C.; Dey, B.; Frontera, A.; Hemming, J.; Helliwell, M.; Gamez, P.; Mukhopadhyay, S. Supramolecular assemblies involving anion−π and lone pair−π interactions: Experimental observation and theoretical analysis. *CrystEngComm* **2011**, *13*, 4519.
(35) Gale, P. A.; Quesada, R. Anion coordination and anion-templated assembly: Highlights from 2002 to 2004. *Coord. Chem. Rev.* **2006**, *250*, 3219−3244.
(36) Cui, K.; Mali, K. S.; Wu, D.; Feng, X.; Müllen, K.; Walter, M.; Feyter, S. de; Mertens, S. F. L. Reversible Anion-Driven Switching of an Organic 2D Crystal at a Solid-Liquid Interface. *Small* **2017**, *13*, 1702379.
(37) Srivastava, A. K.; Praveenkumar, B.; Mahawar, I. K.; Divya, P.; Shalini, S.; Boomishankar, R. Anion Driven [CuIIL2]n Frameworks: Crystal Structures, Guest-Encapsulation, Dielectric, and Possible Ferroelectric Properties. *Chem. Mater.* **2014**, *26*, 3811−3817.
(38) Oliva, L.; Oliva, P.; Galdi, N.; Pellecchia, C.; Sian, L.; Macchioni, A.; Zuccaccia, C. Solution Structure and Reactivity with Metallocenes of AlMe2 F: Mimicking Cation-Anion Interactions in Metallocenium-Methylalumoxane Inner-Sphere Ion Pairs. *Angew. Chem., Int. Ed.* **2017**, *56*, 14227−14231.
(39) Ciancaleoni, G.; Belpassi, L.; Tarantelli, F.; Zuccaccia, D.; Macchioni, A. A combined NMR/DFT study on the ion pair structure of (PR1(2)R2)Au(η2−3-hexyne)BF4 complexes. *Dalton Trans.* **2013**, *42*, 4122−4131.
(40) Zheng, X.-Y.; Xie, J.; Kong, X.-J.; Long, L.-S.; Zheng, L.-S. Recent advances in the assembly of high-nuclearity lanthanide clusters. *Coord. Chem. Rev.* **2019**, *378*, 222−236.
(41) Healy, C.; Schmitt, W. Multicomponent halide templating: The effect of structure-directing agents on the assembly of molecular and extended coordination compounds. *Coord. Chem. Rev.* **2018**, *371*, 67−85.
(42) Trinapakul, M.; Kritayakornupong, C.; Tongraar, A.; Vchirawongkwin, V. Active site of the solvated thiosulfate ion characterized by hydration structures and dynamics. *Dalton Trans.* **2013**, *42*, 10807−10817.
(43) Eklund, L.; Hofer, T. S.; Pribil, A. B.; Rode, B. M.; Persson, I. On the structure and dynamics of the hydrated sulfite ion in aqueous solution–an ab initio QMCF MD simulation and large angle X-ray scattering study. *Dalton Trans.* **2012**, *41*, 5209−5216.
(44) Eklund, L.; Hofer, T. S.; Weiss, A. K. H.; Tirler, A. O.; Persson, I. Structure and water exchange of the hydrated thiosulfate ion in aqueous solution using QMCF MD simulation and large angle X-ray scattering. *Dalton Trans.* **2014**, *43*, 12711−12720.
(45) Eklund, L.; Hofer, T. S.; Persson, I. Structure and water exchange dynamics of hydrated oxo halo ions in aqueous solution using QMCF MD simulation, large angle X-ray scattering and EXAFS. *Dalton Trans.* **2015**, *44*, 1816−1828.
(46) Śmiechowski, M. Anion−water interactions of weakly hydrated anions: Molecular dynamics simulations of aqueous NaBF4 and NaPF6. *Mol. Phys.* **2016**, *114*, 1831−1846.
(47) Elmehdawi, R. M.; El-Kaheli, M. N.; Abuhmaiera, R. G.; Treish, F. A.; Ben Younes, M. E. M.; Bazzicalupi, C.; Guerri, A.; Caneschi, A.;

DOI: 10.1021/jacs.9b01356
J. Am. Chem. Soc. XXXX, XXX, XXX−XXX

Amjad, A. Synthesis, Crystal Structure, and Magnetic Properties of a New Mixed Metal (Co(II), Ni(II)) Cubane. *Materials* **2017**, *10*, 178.
(48) Gahan, L. R.; Henriksen, S. L. Preparation and characterization of di-(μ2-CH3COO-κ2O: O′)-tetrakis[μ3-methoxo-2,4-pentanedionatometal(II, III)] complexes. *Polyhedron* **2015**, *95*, 30−39.
(49) Malpaharia, P.; Pramanik, K.; Costes, J.-P.; Tuchagues, J.-P.; Moulton, B.; Zaworotko, M. J.; Das, B.; Chandra, S. K. Tetranuclear [Mn 2 Co 2], [Mn 2 Fe 2], and [Mn 2 Mn 2] Complexes with Defective Double-Cubane Cores and Phenoxo and Oxo Bridges: Syntheses, Crystal Structures, and Electronic Properties. *Eur. J. Inorg. Chem.* **2014**, *2014*, 3527−3535.
(50) Zhang, S.-H.; Zhao, R.-X.; Li, G.; Zhang, H.-Y.; Zhang, C.-L.; Muller, G. Structural variation from heterometallic heptanuclear or heptanuclear to cubane clusters based on 2-hydroxy-3-ethoxy-benzaldehyde: Effects of pH and temperature. *RSC Adv.* **2014**, *4*, 54837−54846.
(51) Kessler, V. G.; Gohil, S.; Kritikos, M.; Korsak, O. N.; Knyazeva, E. E.; Moskovskaya, I. F.; Romanovsky, B. V. An approach to heterometallic alkoxide-β-diketonate complexes with a M4O4 cubane-like core and new prospects of their application in preparation of solid catalysts. X-ray single crystal study of (Co, Ni)4(acac)4(μ3-OMe)-4(MeOH)4, Co2Ni2(acac)4(μ3-OMe)4(OAc)2 and Mg4(acac)4-(μ3-OMe)4(MeOH)4. *Polyhedron* **2001**, *20*, 915−922.
(52) Lin, P.-H.; Tsui, E. Y.; Habib, F.; Murugesu, M.; Agapie, T. Effect of the Mn Oxidation State on Single-Molecule-Magnet Properties: Mn(III) vs Mn(IV) in Biologically Inspired DyMn3O4 Cubanes. *Inorg. Chem.* **2016**, *55*, 6095−6099.
(53) Kanady, J. S.; Lin, P.-H.; Carsch, K. M.; Nielsen, R. J.; Takase, M. K.; Goddard, W. A.; Agapie, T. Toward models for the full oxygen-evolving complex of photosystem II by ligand coordination to lower the symmetry of the Mn3CaO4 cubane: demonstration that electronic effects facilitate binding of a fifth metal. *J. Am. Chem. Soc.* **2014**, *136*, 14373−14376.
(54) Evangelisti, F.; Güttinger, R.; Moré, R.; Luber, S.; Patzke, G. R. Closer to photosystem II: a Co4O4 cubane catalyst with flexible ligand architecture. *J. Am. Chem. Soc.* **2013**, *135*, 18734−18737.
(55) Evangelisti, F.; Moré, R.; Hodel, F.; Luber, S.; Patzke, G. R. 3d-4f {Co(II)3Ln(OR)4} Cubanes as Bio-Inspired Water Oxidation Catalysts. *J. Am. Chem. Soc.* **2015**, *137*, 11076−11084.
(56) Song, F.; Moré, R.; Schilling, M.; Smolentsev, G.; Azzaroli, N.; Fox, T.; Luber, S.; Patzke, G. R. {Co4O4} and {CoxNi4-xO4} Cubane Water Oxidation Catalysts as Surface Cut-Outs of Cobalt Oxides. *J. Am. Chem. Soc.* **2017**, *139*, 14198−14208.
(57) Olshansky, L.; Huerta-Lavorie, R.; Nguyen, A. I.; Vallapurackal, J.; Furst, A.; Tilley, T. D.; Borovik, A. S. Artificial Metalloproteins Containing Co4O4 Cubane Active Sites. *J. Am. Chem. Soc.* **2018**, *140*, 2739−2742.
(58) Nguyen, A. I.; Wang, J.; Levine, D. S.; Ziegler, M. S.; Tilley, T. D. Synthetic control and empirical prediction of redox potentials for Co4O4 cubanes over a 1.4 V range: implications for catalyst design and evaluation of high-valent intermediates in water oxidation. *Chem. Sci.* **2017**, *8*, 4274−4284.
(59) Nguyen, A. I.; Ziegler, M. S.; Oña-Burgos, P.; Sturzbecher-Hohne, M.; Kim, W.; Bellone, D. E.; Tilley, T. D. Mechanistic Investigations of Water Oxidation by a Molecular Cobalt Oxide Analogue: Evidence for a Highly Oxidized Intermediate and Exclusive Terminal Oxo Participation. *J. Am. Chem. Soc.* **2015**, *137*, 12865−12872.
(60) Liao, R.-Z.; Siegbahn, P. E. M. Possible water association and oxidation mechanisms for a recently synthesized Mn4Ca-complex. *J. Catal.* **2017**, *354*, 169−181.
(61) Hodel, F. H.; Luber, S. Redox-Inert Cations Enhancing Water Oxidation Activity: The Crucial Role of Flexibility. *ACS Catal.* **2016**, *6*, 6750−6761.
(62) Hodel, F. H.; Luber, S. What Influences the Water Oxidation Activity of a Bioinspired Molecular CoII4O4 Cubane? An In-Depth Exploration of Catalytic Pathways. *ACS Catal.* **2016**, *6*, 1505−1517.
(63) Schilling, M.; Hodel, F. H.; Luber, S. Discovery of Open Cubane Core Structures for Biomimetic LnCo3(OR)4 Water Oxidation Catalysts. *ChemSusChem* **2017**, *10*, 4561−4569.
(64) Kanady, J. S.; Tsui, E. Y.; Day, M. W.; Agapie, T. A Synthetic Model of the Mn_3Ca Subsite of the Oxygen-Evolving Complex in Photosystem II. *Science* **2011**, *333*, 733−736.
(65) Zhang, C.; Chen, C.; Dong, H.; Shen, J.-R.; Dau, H.; Zhao, J. A synthetic Mn4Ca-cluster mimicking the oxygen-evolving center of photosynthesis. *Science* **2015**, *348*, 690−693.
(66) Efthymiou, C. G.; Raptopoulou, C. P.; Terzis, A.; Boča, R.; Korabic, M.; Mrozinski, J.; Perlepes, S. P.; Bakalbassis, E. G. A Systematic Exploration of Nickel(II)/Acetate/Di-2-pyridyl Ketone Chemistry: Neutral and Cationic Tetranuclear Clusters, and a Novel Mononuclear Complex. *Eur. J. Inorg. Chem.* **2006**, *2006*, 2236−2252.
(67) Li, Y.-M.; Zhang, J.-J.; Fu, R.-B.; Xiang, S.-C.; Sheng, T.-L.; Yuan, D.-Q.; Huang, X.-H.; Wu, X.-T. Three new cubane-like transition metal complexes of di-2-pyridyl ketone in gem-diol form: Syntheses, crystal structures and properties. *Polyhedron* **2006**, *25*, 1618−1624.
(68) Padhi, S. K.; Sahu, R. Co(II/III) coordinated pyridine alcoholate ligand generated through metal assisted nucleophilic addition to a CO function: Temperature dependent synthesis of a mononuclear complex and a neutral cubane cluster. *Polyhedron* **2008**, *27*, 2662−2666.
(69) Papatriantafyllopoulou, C.; Efthymiou, C. G.; Raptopoulou, C. P.; Vicente, R.; Manessi-Zoupa, E.; Psycharis, V.; Escuer, A.; Perlepes, S. P. Initial use of the di-2-pyridyl ketone/sulfate "blend" in 3d-metal cluster chemistry: Preparation, X-ray structures and physical studies of zinc(II) and nickel(II) cubanes. *J. Mol. Struct.* **2007**, *829*, 176−188.
(70) Proll, P. J.; Sutcliffe, L. H.; Walkley, J. Species of Cobalt(II) in Acetic Acid. Part I. Cobaltous Acetate in the Presence of Water and of Sodium Acetate. *J. Phys. Chem.* **1961**, *65*, 455−460.
(71) Bardan, S.; Aditya, S. *J. Indian. Chem. Soc.* **1955**, *32*, 109.
(72) Katsenis, A. D.; Inglis, R.; Slawin, A. M. Z.; Kessler, V. G.; Brechin, E. K. Transforming the cube: a tetranuclear cobalt(II) cubane cluster and its transformation to a dimer of dimers. *CrystEngComm* **2009**, *11*, 2117−2120.
(73) Katsoulakou, E.; Lalioti, N.; Raptopoulou, C. P.; Terzis, A.; Manessi-Zoupa, E.; Perlepes, S. P. Insights into the role of zinc(II) sites in hydrolytic enzymes: Study of the ZnII/X/(py)2CO (X = Cl-, N3-, SO42-;) reaction systems. *Inorg. Chem. Commun.* **2002**, *5*, 719−723.
(74) Bickley, R. I.; Edwards, H. G. M.; Rose, S. J.; Gustar, R. A raman spectroscopic study of nickel(II) acetate, Ni(CH3COO)2 and its aqueous and methanolic solutions. *J. Mol. Struct.* **1990**, *238*, 15−26.
(75) La Ganga, G.; Nardo, V. M.; Cordaro, M.; Natali, M.; Vitale, S.; Licciardello, A.; Nastasi, F.; Campagna, S. A functionalized, ethynyl-decorated, tetracobalt(III) cubane molecular catalyst for photo-induced water oxidation. *Dalton Trans.* **2014**, *43*, 14926−14930.
(76) Berardi, S.; La Ganga, G.; Natali, M.; Bazzan, I.; Puntoriero, F.; Sartorel, A.; Scandola, F.; Campagna, S.; Bonchio, M. Photocatalytic water oxidation: tuning light-induced electron transfer by molecular Co4O4 cores. *J. Am. Chem. Soc.* **2012**, *134*, 11104−11107.
(77) McCool, N. S.; Robinson, D. M.; Sheats, J. E.; Dismukes, G. C. A Co4O4 "cubane" water oxidation catalyst inspired by photosynthesis. *J. Am. Chem. Soc.* **2011**, *133*, 11446−11449.
(78) Kirchhoff, B.; Rau, S.; Streb, C. Detecting and Preventing the Formation of Photosensitizer-Catalyst Colloids in Homogeneous Light-Driven Water Oxidation. *Eur. J. Inorg. Chem.* **2016**, *2016*, 1425−1429.

DOI: 10.1021/jacs.9b01356
J. Am. Chem. Soc. XXXX, XXX, XXX−XXX